Mechanical tugging force regulates the size of cell–cell junctions

Zhijun Liu[a,1], John L. Tan[b,1], Daniel M. Cohen[a,1], Michael T. Yang[a], Nathan J. Sniadecki[a], Sami Alom Ruiz[a], Celeste M. Nelson[b], and Christopher S. Chen[a,b,2]

[a]Department of Bioengineering, University of Pennsylvania, Philadelphia, PA 19104; and [b]Department of Biomedical Engineering, Johns Hopkins School of Medicine, Baltimore, MD 21205

Edited by Shu Chien, University of California, San Diego, La Jolla, CA, and approved March 31, 2010 (received for review December 17, 2009)

Actomyosin contractility affects cellular organization within tissues in part through the generation of mechanical forces at sites of cell–matrix and cell–cell contact. While increased mechanical loading at cell–matrix adhesions results in focal adhesion growth, whether forces drive changes in the size of cell–cell adhesions remains an open question. To investigate the responsiveness of adherens junctions (AJ) to force, we adapted a system of microfabricated force sensors to quantitatively report cell–cell tugging force and AJ size. We observed that AJ size was modulated by endothelial cell–cell tugging forces: AJs and tugging force grew or decayed with myosin activation or inhibition, respectively. Myosin-dependent regulation of AJs operated in concert with a Rac1, and this coordinated regulation was illustrated by showing that the effects of vascular permeability agents (S1P, thrombin) on junctional stability were reversed by changing the extent to which these agents coupled to the Rac and myosin-dependent pathways. Furthermore, direct application of mechanical tugging force, rather than myosin activity per se, was sufficient to trigger AJ growth. These findings demonstrate that the dynamic coordination of mechanical forces and cell–cell adhesive interactions likely is critical to the maintenance of multicellular integrity and highlight the need for new approaches to study tugging forces.

adherens junction | mechanotransduction | myosin | PDMS | traction force

Cells generate contractile forces against their substratum and on surrounding cells primarily through myosin-generated tension in the actin cytoskeleton (1, 2). Studies in model organisms have revealed that this actomyosin activity is critical for tissue morphogenesis and dynamic regulation of cell–cell contacts. During gastrulation, apical constriction and an inward displacement of cell–cell junctions is driven by myosin II activity, allowing cells of the ventral furrow to invaginate (3, 4). Additionally, myosin II is essential for stereotypical cell shape changes and redistribution of cell–cell contacts that accompany tissue extension/expansion by cell intercalation in both Drosophila (5, 6) and Xenopus models (7, 8). Maintenance of cell–cell junctions in embryogenesis also appears to depend on myosin as loss of myosin heavy chain IIA disrupts E-cadherin and beta-catenin recruitment to cell–cell junctions and impairs cell–cell adhesion in embryoid bodies (9). Together, these studies demonstrate a requirement for myosin II in the organization of cell–cell junctions and imply that myosin-dependent forces may play a role in regulating cell–cell adhesion.

Among the different types of cell–cell junctions, the adherens junctions (AJ), in particular, appear sensitive to changes in myosin-dependent cytoskeletal tension. Inhibition of Rho kinase, MLCK, myosin ATPase activity or expression interferes with the growth and maintenance of adherens junctions in several systems (10–15). E- and N-cadherin cluster into focal adhesion-like structures when cells are plated on cadherin-coated substrates, and this clustering requires actomyosin contractility (14, 16, 17). Yet, unlike the mechanosensitivity of focal adhesions (18), force-dependent assembly of cadherins cell–cell junctions is not well established. Nevertheless, focal adhesions and AJs depend on the actin cytoskeleton for anchoring to the matrix or neighboring cells, respectively, and to withstand substantial forces (19).

To test the functional importance of forces at AJs, various systems have been developed to load cell–cell adhesions using atomic force microscopy (AFM), pipettes, or magnetically trapped beads (20–27). Pulling beads bound to cadherins with ~1–150 pN forces are sufficient to elicit cellular signaling and actin assembly (20, 24, 27). Force-induced breakage of E-cadherin bonds, however, requires much stronger forces (~200 nN) (23). While these studies describe a wide range of forces that cells can experience at cell–cell adhesions, these studies fail to capture the role of endogenous, cell-generated forces experienced at the AJ.

Here we describe a method using microfabricated force sensors that reports quantitatively on both the force applied to the cell–cell contact and AJ size. We find that endothelial cells generate substantial forces (up to ~120 nN) that pull normal to the face of the cell–cell contact, designated as the intercellular tugging force. Furthermore, we demonstrate a robust correlation between AJ size and tugging force and reveal that both junctional parameters are directly responsive to myosin activity. This actomyosin contractility cooperates with a Rac-mediated pathway to determine the ultimate size of AJs. Furthermore, acute stimulation with RhoA or the application of exogenously pulling forces initiates a rapid AJ growth. These findings demonstrate that AJs undergo mechanically induced growth in response to loading and suggest that cell-generated forces can influence the architecture of tissues by regulating the strength of cell–cell adhesions.

Results

A Microfabricated Force Sensor For Measuring Cell–Cell Tugging Force. To measure tugging force, we retooled a previously described approach that uses an array of elastomeric microneedles to measure traction forces (28) (Fig. 1 *A–C* and Eq. **1** in Fig. 1*B*). Cells exist in a quasi-static equilibrium where net force sums to zero (28, 29) (n.b., an imbalance of 1 nN would accelerate a 10 ng cell at 100 m/s^2). For a cell in contact with a neighbor, the net force encompasses both traction forces and the intercellular tugging force experienced at the cell–cell contact (Fig. 1 *D–F*). Because the net force remains zero, the intercellular tugging force, F_c, is equal in magnitude and opposite in direction to the measured net traction force reported by the microneedle array (Fig 1*F* and Eq. **2** in Fig. 1*F*). This approach relies on the formation of a single contacting interface between two cells; calculating forces across multiple cell–cell contacts is mathematically insoluble. Whereas

Author contributions: Z.L., J.L.T., D.M.C., M.T.Y., S.A.R., C.M.N., and C.S.C. designed research; Z.L., J.L.T., D.M.C., M.T.Y., and S.A.R. performed research; Z.L., J.L.T., D.M.C., M.T.Y., and C.M.N. contributed new reagents/analytic tools; Z.L., J.L.T., D.M.C., M.T.Y., and S.A.R. analyzed data; and Z.L., D.M.C., N.J.S., and C.S.C. wrote the paper.

The authors declare no conflict of interest.

This article is a PNAS Direct Submission.

[1]Z.L., J.L.T., and D.M.C. contributed equally to this paper.

[2]To whom correspondence should be addressed. E-mail: chrischen@seas.upenn.edu.

This article contains supporting information online at www.pnas.org/lookup/suppl/doi:10.1073/pnas.0914547107/-/DCSupplemental.

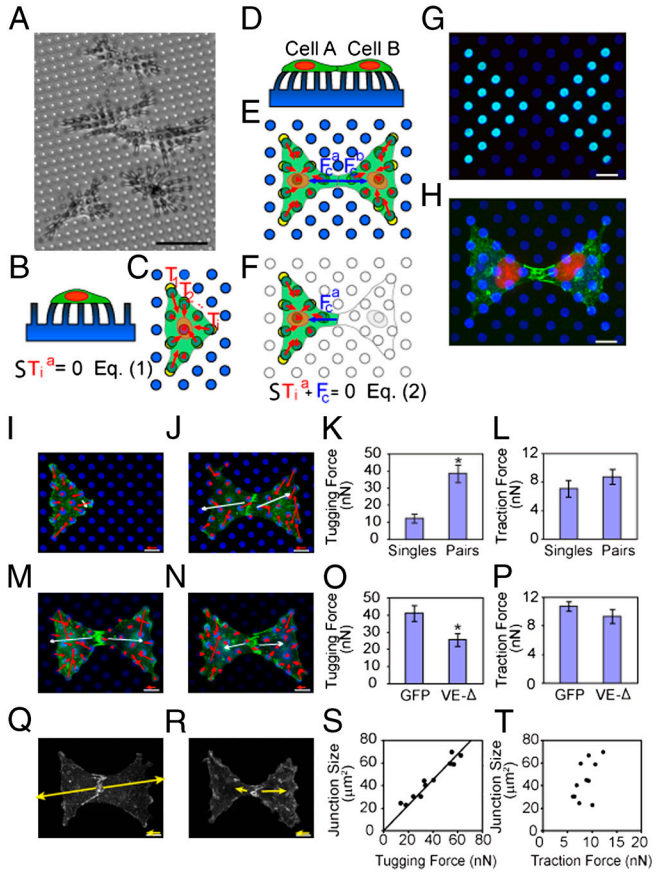

Fig. 1. An approach to measure tugging forces (*A*) Endothelial cells exert contractile forces that strongly deflect underlying microneedles (phase contrast image; scale bar, 50 μm). (*B* and *C*) The vector sum of individual traction forces, T_n, (*Red Arrows*) exerted by a cell is zero (Eq. **1**) (28, 29). (*D* and *E*) For a pair of contacting cells, the net force encompasses both traction forces (*Red Arrows*) and the intercellular tugging force, F_c, (*Blue Arrows*). (*F*) The intercellular tugging force is equal in magnitude and opposite in direction to the measured net traction force reported on the microneedle array (Eq. **2**). Vector F_c plotted over cell A is defined as the net tugging force that cell A is exerting on cell B at the cell–cell contact. Cell B is expected to pull on cell A with an equal and opposite force. (*G* and *H*) Cells were constrained to a bowtie pattern using microcontact printing of fibronectin (*Cyan*) (*G*) and formation of adherens junctions in green (anti-β-catenin, *H*). Microneedles and cell nuclei were counterstained with DiI (*Blue*) and DAPI (*Red*), respectively. Scale bar, 10 μm. (*I* and *J*) Representative force vector plots of single (*I*) and paired (*J*) cells. Force vectors are plotted as arrows showing the direction of force and magnitude (arrow length; reference arrow for 10 nN shown above scale bar). Individual traction forces are shown in red and tugging force is shown in white. Small, force imbalances are observed due to uncertainties in microneedle deflection measurements. The error in the vector sum of individual traction forces equals the error of the individual forces multiplied by the square root of the number of tractions. The microneedles typically have an error of ±3 nN, and cells span on average 15 microneedles, leading to an expected noise level of 12 nN in the determination of F_c. (*K*) Average F_c experienced in bowtie pairs of HPAECs. * $p < 0.05$ indicates comparison against single cells. (*L*) Average traction force per microneedle was similar in singlet or contacting cells. (*M–O*) Tugging forces require coupling between VE-cadherin and the actin cytoskeleton. Cells expressing adeno-VE-Δ, a truncated VE-cadherin mutant lacking the β-catenin binding domain (residues 703–784), form adherens junctions (anti-β-catenin, *Green*, *N*) but show greatly diminished tugging force compared to adeno-GFP infected cells (*M* and *O*). * $p < 0.05$ indicates comparison against GFP. (*P*) Average traction force per microneedle was unaffected by VE-Δ expression. (*Q* and *R*) AJ (anti-β-catenin) in HPAECs are heterogeneous in size. Tugging force is shown in yellow. (*S*) AJ size is linearly correlated with F_c, with a correlation coefficient $R^2 \approx 0.9$. Each data point represents one pair of cells. (*T*) AJ size is not correlated with the average traction force per microneedle. Error bars on all graphs denote standard error of the mean.

random seeding yields few cells forming a single cell–cell contact, efficient pair formation was obtained by bowtie micropatterns (28) (Fig. 1 *G* and *H*).

To determine whether cells exert a measurable intercellular F_c, we assayed forces in endothelial cells seeded as singlets or in contacting pairs on the microneedle substrates (Fig. 1 *I* and *J*). In contacting cells, but not singlets, a substantial F_c (~40 nN), oriented roughly normal to the face of the AJ, was observed and was sustained over several hours (Fig. 1 *J* and *K*). No difference in average traction force per microneedle was observed between singlet and contacting cells (Fig 1*L*). To confirm that the observed F_c reflects contractile forces transmitted to the AJ, we tested whether decoupling VE-cadherin from the actin cytoskeleton perturbed F_c. Expression of a mutant VE-cadherin deficient in β-catenin binding (deletion of residues 703–784) (30) decreased F_c to nearly half the level measured in GFP expressing control cells (Fig. 1 *M–O*), whereas traction forces remained similar (Fig. 1*P*). Thus, tugging forces are applied to the AJ, and the transmission of such forces requires that VE-cadherin be anchored to the catenin complex.

AJ size (area of β-catenin staining) was heterogeneous in the bowtie patterns (Fig. 1 *Q* and *R*). Interestingly, the size of AJs and the magnitude of F_c were linearly correlated, resulting in an apparent constant stress of ~1 nN/μm^2 (Fig. 1*S*). Traction force per microneedle, a measure of global cellular contractility, was uncorrelated with AJ size, indicating that changes in AJ size are specific to changes in local tugging force (c.f. Fig. 1*S* vs. *T*).

Myosin II-Dependent Tugging Forces Regulate AJ Assembly. These data suggested the possibility that cell–cell junction assembly, much like focal adhesion assembly, is a force-dependent process. To test this hypothesis, we antagonized cytoskeletal tension by treatment with Y-27632 (a Rho kinase inhibitor) or blebbistatin (myosin II ATPase inhibitor). Both inhibitors substantially decreased average traction force and F_c and caused a reduction in AJ size, preserving the linear relationship between F_c and junctions (Fig. 2 *A–D*). Likewise, siRNA-mediated knockdown of either myosin IIA or IIB decreased traction force, F_c, and junction size (Fig. 2 *A–C* and *E*).

These data are consistent with a reported requirement for myosin in maintaining adherens junctions (9, 10, 12–15). However, whether increasing myosin-mediated tension promotes AJ assembly is largely untested. We therefore assayed the effects of the tension-inducing drugs nocodazole and calyculin-A in our system. Both agents significantly increased traction force, F_c, and AJ assembly (Fig. 2 *B*, *C*, and *F*), supporting a role for tension-induced AJ assembly. To achieve direct molecular targeting of myosin, we infected cells with lentivirally encoded phosphomimetic mutants (T18D, S19D) of myosin regulatory light chain (MLC). Phosphomimetic MLC, but not wild-type MLC, dramatically enhanced average traction force and F_c and induced more expansive AJs (Fig. 2 *B*,*C*, and *G*).

Remarkably, compiling all of our studies with tension manipulations revealed a general relationship between AJ size and F_c that spanned a wide range of AJ areas (~7–87 μm^2) and F_c (~7–120 nN) (Fig. 2*H*). Using moving average and bootstrap methods to calculate the mean and 99% percent confidence interval, one can appreciate a linear relationship between AJs and F_c in the smaller force/AJ regime, whereas the response of AJ begins to saturate at forces higher than ~70 nN, suggesting an upper limit for mechanosensitive growth of AJs.

To examine whether this force–AJ relationship can be generalized, we characterized the response of AJs in conventional monolayers to tension manipulations. Consistent with the bowtie system, treatment of monolayers with tension antagonists reduced AJ levels as compared to unstimulated cells (Fig. 2 *I–K*). Conversely, upregulation of tension increased the size of AJs in the monolayers (Fig. 2 *I*,*J*, and *L*). Thus, tugging forces appear to

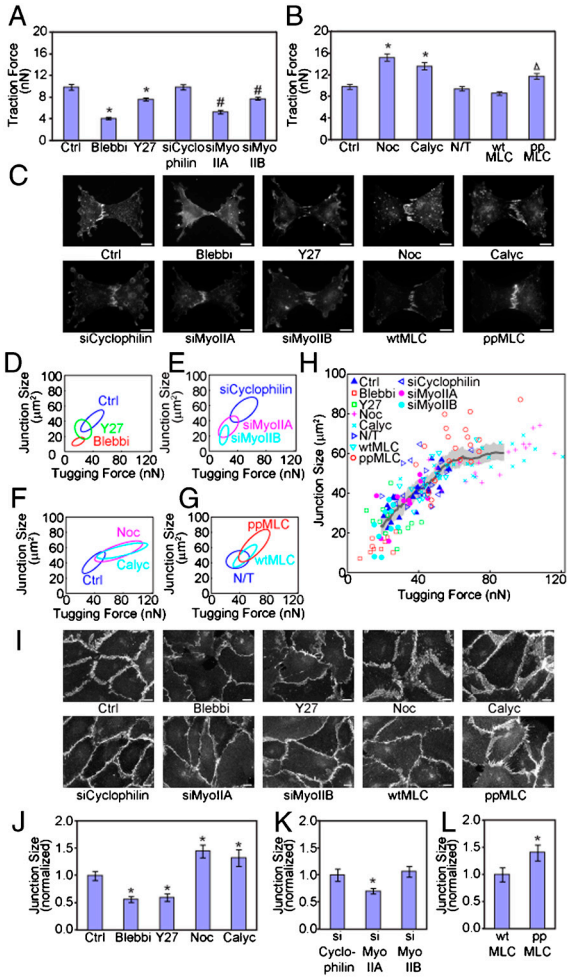

Fig. 2. Tugging force regulates the size of adherens junctions. (*A* and *B*) Tension antagonists and agonists modulate average traction force per microneedle and F_c. The following antagonists were used: blebbistatin (30 μM, Blebbi), Y27632 (25 μM, Y27), siRNA against myosin IIA (siMyoIIA), myosin IIB (siMyoIIB). Tension agonists included nocodazole (1 μM, Noc) calyculin-A (1nM, Calyc), lentivirally encoding phosphomimetic light chain (ppMLC). Control conditions included vehicle control (Ctrl), control siRNA (siCyclophilin), no treatment (N/T), or lentiviral wild-type MLC (wtMLC). * $p < 0.05$ indicates comparison against vehicle control, # $p < 0.05$ indicates comparison against control siRNA, and Δ $p < 0.05$ indicates comparison against wtMLC. (*C*) AJ size is regulated by changes in actomyosin-mediated tension. Bowtie pairs exposed to the conditions in (*A* and *B*) and stained for β-catenin. (*D–G*) Relationship between AJ size and F_c. Inhibition of F_c by blebbistatin, Y27632 (*D*) or treatment with siRNA against myosin II A or B (*E*) leads to reduced junction size, whereas elevated F_c following stimulation with nocodazole, calyculin-A (*F*), or infected with lentivirus encoding phosphomimetic mutants (*G*) increased junction size. AJ size and F_c measurements (at least 10 bowtie pairs per condition) were clustered and plotted as an elliptical fit (*D–G*). Statistical significance between conditions is reported in Table S1. (*H*) A scatter plot showing the correlation between AJ size and F_c across all conditions. (*I–L*) Tension manipulations affect AJs in monolayers. Immunofluorescence images showing changes in AJs (anti- β -catenin) in HPAECs monolayers exposed to tension-manipulating conditions (*I*). Quantification of monolayer junctional response (*J–L*). * $p < 0.05$ indicates comparison against control monolayers: Ctrl (*J*), siCyclophilin (*K*), or wtMLC (*L*). All scale bars are 10 μm. Error bars denote standard error of the mean.

regulate junction size, regardless of experimental culture conditions (bowties versus monolayers).

Vasoactive Compounds Regulate AJ Size Through Rho/Force- and Rac-Dependent Pathways. While the aforementioned tension manipulations reveal an important linkage between myosin activity, tugging forces, and regulation of AJ size, these treatments lack a physiological context. We hypothesized that physiological stimuli may also control cell–cell junction homeostasis in endothelium through tugging forces. Inflammatory agents such as thrombin have been proposed to disrupt cell–cell contacts through increased RhoA-mediated myosin-generated contraction (31), which represents a counterexample to the stimulatory effects of myosin contractility on AJs observed here (Fig. 2). Sphingosine-1-phosphate (S1P), another vasoactive compound, appears to strengthen cell–cell contact (32) at a concentration that does not impact cellular contractility (33), hinting at the possibility of a force-independent modulation of junction size.

Application of thrombin or S1P to monolayers induced the expected disruption or enhancement of AJ assembly, respectively (Fig. 3 *A* and *B*). To clarify how these permeability agents impact AJs, we assayed AJs and F_c in the bowtie-microneedle system. Traction force and F_c increased in response to thrombin without a concomitant increase in junction size (Fig. 3 *C–E*), resulting in a precipitous rise in mechanical stress at the junction (from ∼1 to ∼8 nN/μm^2). In fact, cell–cell contacts were either disrupted by thrombin or resulted in residual AJs that were shorter, fainter, and less distinct relative to controls (Fig. 3*B*). In contrast, S1P triggered AJ expansion in a tortuous path across the cell–cell contact, without affecting F_c (Fig. 3 *D* and *E*), and thus reduced junctional stress (to ∼0.5 nN/μm^2).

The uncoupling of junction size and F_c in S1P and thrombin-treated cells implies the existence of a mechanism of AJ growth that is independent of F_c or one that modulates the coupling of AJ growth to F_c. One such mechanism could be the regulation of AJs by the Rac1 GTPase. Activated Rac1 is localized to sites of nascent cell–cell contact (15) and is implicated in regulating the assembly kinetics and strength of AJs (34). Importantly, Rac1 is activated in response to S1P (33, 35), and this activation is required for S1P-mediated junctional assembly (35). We therefore investigated the relationship of Rac1 activity to AJ size and tugging forces in the presence of vasoactive compounds. Measurements of Rac and RhoA activity (an upstream mediator for myosin/tension driven responses) revealed that thrombin robustly activated RhoA, while suppressing Rac activity (Fig. 3*F*). In contrast, S1P specifically upregulated Rac activity, while leaving RhoA unperturbed (Fig. 3*F*). These data suggested a direct correlation between junction size and Rac activity. Rac activity can be antagonized using NSC23766, which prevents the interaction of Rac1 and its upstream activators Tiam1 and Trio (36). To test whether Rac activity was required for S1P-mediated junctional assembly, HPAECs were challenged with S1P in the presence of NSC23766 (10 μM). NSC23766 abolished S1P-induced AJ assembly (Fig. 3 *H* and *I*), demonstrating that Rac activation contributes to junctional growth.

We then tested whether changes in Rho and Rac activity also contributed to thrombin-induced junctional disassembly. Pretreatment with Y27632 inhibited the thrombin-induced increase in traction forces and F_c and prevented the disruption of junctions (Fig. 3 *G–I*). Remarkably, expression of a constitutively active Rac mutant (RacV12) (37) prevented thrombin-induced disassembly (Fig. 3 *G–I*). These finding suggest that Rac activity and tugging force are both important determinants in the response of AJs to vasoactive compounds.

Rac Activity and Tugging Force Cooperate to Regulate AJ Size. To examine whether Rac activity indeed cooperates with F_c to regulate AJ size, we examined the effect of jointly manipulating tension and Rac activity. RacV12 alone induced junction assembly without altering F_c, suggesting AJ growth does not require an increase in basal F_c. However, treatment of RacV12 cells with blebbistatin partially inhibited AJ assembly, demonstrating that Rac-induced junctions remained dependent on baseline tugging forces (Fig. 3 *J–L*). Conversely, with the Rac antagonist, NSC23766, attenuated the ability of phosphomimetic myosin to promote

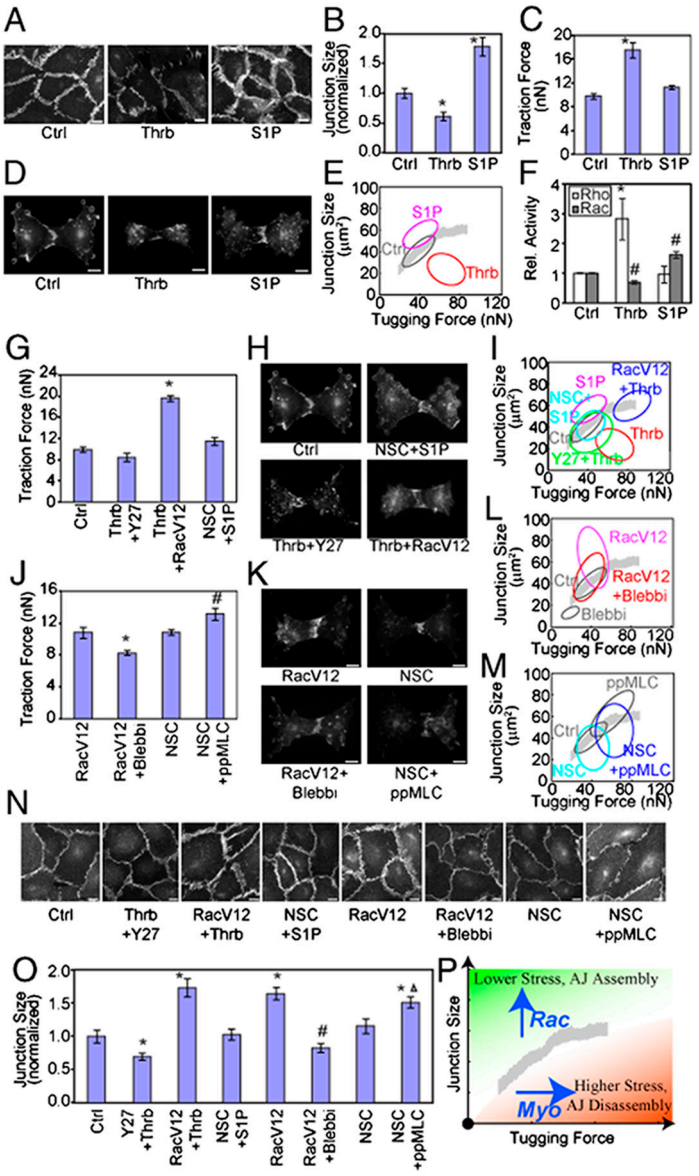

Fig. 3. Modulation of force-AJ relationship by soluble factors. (*A* and *B*) Vasoactive compounds S1P and thrombin coordinately upregulate and downregulate adherens junctions. (*A*) Monolayers exposed to vehicle only (Ctrl), thrombin (0.1 μM, Thrb), or S1P (1 μM, S1P) show S1P-induced AJ growth and thrombin-induced AJ disassembly (anti-β-catenin staining). (*B*) Quantification of changes in AJs in monolayer cultures shown in *A*. * $p < 0.05$ indicates comparison against control. (*C*) Thrombin, but not S1P, induces cellular tension. Bar graph showing average traction force per microneedle reported in bowtie pairs stimulated with vasoactive compounds. (*D* and *E*) Effects of thrombin and S1P on junctional size-tugging force relationship. S1P and thrombin alter AJ formation (anti-β-catenin) in bowtie pairs (*D*). Relationship between AJ and F_c data plotted as an elliptical fit (*E*). The trend band and control condition from Fig. 2 are replotted here for reference. (*F*) RhoA and Rac1 activity assay for Thrombin and S1P using Rho G-LISA and Rac G-LISA kits, respectively. *, # $p < 0.05$ indicates comparison against baseline RhoA (*) or Rac (#) activity. (*G*) Manipulations of Rac activity do not alter cellular tension, as assayed by average traction force per microneedle. In contrast, inhibition of Rho kinase (Y27632, 25 μM) blocks thrombin-induced tension. * $p < 0.05$ indicates comparison against control. (*H* and *I*) Altering the coupling of S1P and thrombin to Rac and tension-dependent pathways reverse the effects of these vasoactive compounds on junctions. S1P-induced AJ growth is inhibited by treatment with NSC23766 (10 μM), whereas thrombin-induced AJ disassembly is blocked by expression of constitutively active Rac (RacV12). AJ junctions visualized by β-catenin localization (*H*). Decoupling thrombin from cellular tension or forcibly linking it to constitutively active Rac restores the linear relationship between AJ and tugging force. Similarly, inhibition of Rac1 with NSC23766 restores the normal AJ-tugging force balance in S1P-stimulated cells. (*J*) Myosin-manipulation regulates cellular tension independently of Rac activity levels. Blebbistatin (30 μM) downregulates average traction force per microneedle even in the presence of RacV12, whereas phosphomimetic myosin upregulates average traction force, even in the context of reduced Rac activity (NSC23766 treatment). * $p < 0.05$ indicates comparison against RacV12; and # $p < 0.05$ indicates comparison against NSC23766. (*K*– *M*) Interdependence of Rac-induced and tension-induced AJ assembly. Inhibition of myosin activity (blebbistatin, 30 μM) reduced the growth of AJs stimulated by constitutively active Rac (RacV12). Loss of Rac activity reduced the growth of AJs stimulated by phosphomimetic myosin. AJs visualized by β-catenin localization. (*L* and *M*) Effects of double Rac/myosin manipulations in *J* on AJ-T_c relationship. (*N* and *O*) Rac and tension-dependent pathways control the size of AJs in monolayer culture. Representative immunofluorescent micrographs of monolayers of cells exposed to the treatments in (*G*–*M*). AJs are visualized by β-catenin staining (*N*). Quantification of changes in junction size in monolayers (*O*). * $p < 0.05$ indicates comparison against Ctrl; # $p < 0.05$ indicates comparison against RacV12; and Δ $p < 0.05$ indicates comparison against NSC23766. (*P*) Schematic of how myosin-mediated tugging force and Rac activity coordinate to determine the ultimate size and stability of AJs. We suggest three general regimes: a low stress regime (*Shaded Green*) wherein high Rac activity support AJs assembly independently of tugging force, a moderate stress regime (*White Region*) wherein Rac activity and myosin-mediated tugging force coordinate to mediate mechanosensitive growth of AJs, and a high stress regime (*Shaded Red*) wherein high tugging forces/myosin activity initiate breaking/disassembly of junctions due to insufficient Rac-mediated junction assembly. All scale bars are 10 μm. Error bars on all graphs denote standard error of the mean. Statistical significance between conditions *E*, *I*, *L*, and *M* is reported in Table S1.

junction growth (Fig 3 *J*,*K*, and *M*) further supporting the hypothesis that Rac activity is permissive for force-induced junction growth. Again, similar effects were observed in monolayers as in our bowtie system, suggesting that these relationships between Rho, Rac, and junction assembly are conserved in more general settings (Fig. 3 *N* and *O*). Together, these studies suggest a model whereby Rho-mediated myosin activity generates tugging forces, and Rac mediates the ability of AJs to assemble in response to those forces (Fig. 3*P*).

Tugging Force Is Necessary and Sufficient for Rho-dependent AJ Assembly. While the aforementioned studies argue that tugging forces cause AJ assembly, the reliance on myosin manipulations cannot preclude indirect effects of these manipulations on cortical actin assembly. Moreover, single end-point studies do not provide any insights into the temporal coupling of these phenomena. To address these shortcomings, we characterized the dynamic response of AJs to the acute stimulation of contractility in one cell of a bowtie pair. Microinjection of the activated RhoA-Q63L produced an immediate and robust increase in both traction forces (the noninjected cell shows a delayed response) and F_c (Fig. 4 *B* and *D*), whereas no effect was observed upon microinjection of wild-type RhoA (Fig. 4 *A* and *C*). Importantly, RhoA-Q63L triggered AJ growth, as revealed by GFP-VE-cadherin localization, within minutes of rising F_c (Movies S1 and S2 and Fig. 4 *E* and *F*), in a tension-dependent manner (Movies S1 and S2 and Fig. 4*F*). To confirm whether mechanical force is truly sufficient to promote junction growth, we also placed a micropipet onto one of the cells within the bowtie pair and pulled to apply an exogenous tugging force (Movies S3 and S4 and Fig. 4*G*). Mechanical loading of the cell–cell junction also promoted VE-cadherin assembly within several minutes of tugging (Movies S3 and S4 and Fig. 4 *G* and *H*). These data provide direct evidence that adherens junction assembly responds to cell–cell forces.

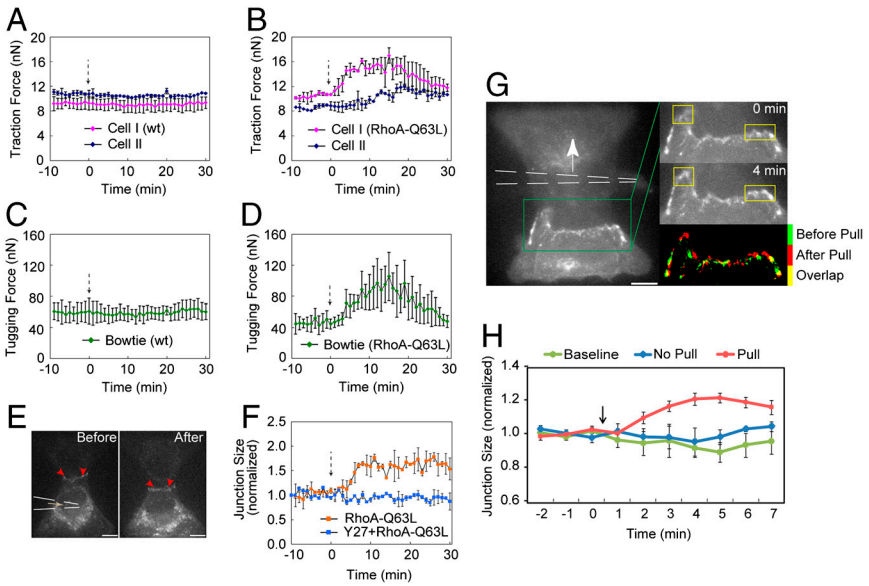

Fig. 4. Microinjection of constitutively active RhoA and direct mechanical tugging leads to junction assembly. (*A* and *B*) Time-series plots showing enhancement of traction force in response to microinjection of constitutively active Rho protein (RhoA-Q63L) (*B*) but not wild-type Rho protein (wt) (*A*) for each of the two cells in bowtie pairs. Dotted arrow indicates the time point of microinjection, and only Cell I (*Purple Line*) was microinjected. Whiskers show the range of traction force observed in two independent bowtie movies. (*C* and *D*) Microinjection of RhoA-Q63L (*D*) but not wild-type Rho protein (*C*), acutely boosts tugging forces for each of the two cells in bowtie pairs. Dotted arrow indicates the time point of microinjection. Whiskers show the range of two microinjected bowtie pairs across all time points. (*E*) Representative image frames showing assembly of GFP-VE-cadherin following microinjection of RhoA-Q63L, 10 minutes before and 16 minutes after microinjection, respectively. Dotted white lines indicate the location of the pipette and the red arrowheads point to locations of increased AJ size. Scale bar is 10 μm. (*F*) RhoA-Q63L induced AJ assembly in a tension-dependent manner. The RhoA-microinjected pairs (*Orange Squares*) showed an increase in junction size while pretreatment with Y27632 (25 μM) blocked this effect (*Blue Squares*). Dotted arrow indicates the time point of microinjection. Whiskers show the range of two replicated experiments across all time points. (*G*) Exogenous tugging force stimulated VE-cadherin assembly. Fluorescence micrograph of GFP-VE-cadherin distribution prior to micropipet-mediated mechanically tugging of the cell–cell junction. Dotted white lines indicate the location of the pipette and the white arrow points to the direction of pipette movement. Region of interest (*Green Box*) shows distribution of junctional VE-cadherin before (0 min) and after tugging (4 min), pseudocolored green and red, respectively in the overlay image. Yellow boxes denote the regions of the AJ showing the strongest cadherin recruitment. Scale bar is 10 μm. (*H*) Quantification of AJ growth in response to mechanical tugging. AJ size of bowtie pairs over 10 min intervals plotting for baseline (*Green Line*), with pipette on top of the cell but no tugging (*Blue Line*), or before and after tugging one cell of the bowtie (Red). Black arrow indicates the time point of tugging with the micropipet. Whiskers show the standard error of the mean across six independent experiments.

Discussion

Tugging forces are critical in morphogenesis, mechanical integrity, and in generating gradients of mechanical stresses to regulate patterns of cell function (38–40). Prior research has emphasized the role of externally applied forces necessary in breaking or remodeling cell–cell adhesions (23, 24, 27). Herein we demonstrate an approach to directly measure endogenous stresses generated between cells and illustrated that such tugging forces induce junction growth. Tugging force measurements were facilitated by bowtie patterns to constrain cells to a single contacting interface. Because cell shape and cell–cell contact can alter cytoskeletal organization (41, 42), results using the bowtie configuration may not extend to other settings. Yet many of the observed responses of tugging forces and AJ size in bowties appear to be similar in monolayers. Nevertheless, further characterization of tugging forces in different settings remains an important challenge.

Interestingly, AJs adjust dynamically in response to changes in tugging forces. While a requirement for myosin II in maintenance of basal AJ size is well established (10–15), here we show that activated myosin as well as direct application of exogenous tugging forces induces AJ assembly that occurs within minutes of force application. Our data suggest that mechanosensitive growth is a fundamental mechanism for controlling AJ size and is strikingly similar to what occurs at focal adhesions (18). As postulated for focal adhesions, the physiologic consequences of this force-dependent AJ growth are likely twofold. First, force-induced assembly dissipates mechanical stress and may protect the junction against breakage (43). Second, AJs are molecular signaling hubs (44), and force-induced junction assembly may trigger signaling that contributes to the process of mechanotransduction.

Although the mechanism of tugging-force-induced AJ growth remains unknown, several models can be considered. In the "zipper" model, localized myosin activation at the expanding edges of cell–cell contacts increases the surface area of cell–cell contact, thus increasing the likelihood of transcadherin interactions (15). An alternative push-pull model suggests that nascent cadherin interactions develop at filopodial-like protrusions along the cell–cell contact (45), and these filopodial-like protrusions are stabilized by the application of normal tugging forces (46). In either model, junction growth is predicated on membrane protrusive activity, a Rac-dependent process (47).

In this context, it is especially interesting that we observe that force-dependent growth of AJs depends, in part, on Rac1 activity. Rac1 may play a permissive role in force-dependent junction growth by supporting the membrane protrusion activity implicated in the aforementioned zipper or push-pull models. Alternatively, Rac1 may play a direct role in force-mediated actin polymerization (16, 22, 48), cytoskeletal coupling of VE-cadherin (16, 25, 48), or regulation of catenin function (49). Attenuation of these Rac1-dependent processes may abrogate intracellular signaling required for force-induced junction assembly. Interestingly, we have also implicated the downregulation of Rac1 in force-dependent junctional disassembly induced by thrombin. Coordinate upregulation of tugging force (ppMLC) and downregulation of Rac (NSC23766) did not, however, trigger AJ disassembly. While thrombin may suppress Rac more potently than NSC23766, thrombin-mediated disassembly may require additional biochemical events such as thrombin-induced phosphorylation of catenins (50), in addition to reciprocal up/downregulation of tugging force and Rac1 activity. Regardless, our findings

underscore the complex and adaptive interplay between signaling, mechanical forces, and junctional structure.

Not only do tugging forces regulate cell–cell adhesions, but cell–cell adhesions can, in turn, trigger many signals including the Rho GTPases to regulate cellular mechanics (41). This interplay between force and adhesion highlights how channeling of actomyosin-generated traction and tugging forces at the cell–matrix and cell–cell interface provide a means to dynamically reorganize cell–matrix and cell–cell adhesions locally, as well as the architecture of tissues globally, and further support coordinated crosstalk between the two mechanical interfaces of the cell with its external environment. Understanding the balance between forces across each of these two interfaces ultimately may help to explain multicellular reorganizations such as occur during tissue morphogenesis and demonstrates the need for better approaches to describe these forces.

Materials and Methods

The experimental methods and protocols are described briefly; a detailed description is included in *SI Text*. PDMS microneedle array substrates were fabricated as in Tan et al. (28). Bowtie patterns had a total area of 1600 μm^2. Microneedle deflections were calculated using Matlab to determine the displacement of the centroid of the microneedle at the tip (see *SI Text*). Forces were then computed via a known spring constant of the microneedle, (32 nN/μm). AJ size was quantified based on thresholded anti-β-catenin fluorescence images and validated against a more rigorous volumetric analysis (Fig. S1). Mean pixel intensity of staining was measured, to confirm that increases in AJ area did not occur at the expense of intensity of staining (Fig. S1). Ellipse-fitting was performed with a least-squares ellipse algorithm in Matlab (51). The trend band of junction size at different tugging force levels is plotted as a moving average (*Darker Gray Line*) ±99% Confidence Interval (CI, *Lighter Gray Region*) using Matlab.

ACKNOWLEDGMENTS. GFP-VE-cadherin and RacV12 adenovirus were generous gifts of S. Shaw/F. Luscinskas and A. Ridley respectively; K. G. Birukov, R. A. Desai, J. G. N. Garcia, D. M. Pirone, A. Popel, D. Reich, and L. H. Romer provided helpful discussions. This work was supported in part by grants from the National Institutes of Health (EB00262, EB08396, GM74048, HL73305, HL90747), the Material Research Science and Engineering Center, and the Center for Engineering Cells and Regeneration of the University of Pennsylvania. J.L.T. and C.M.N received support from the Whitaker Foundation. Ruth L. Kirschstein National Research Service Awards supported D.M.C. and N.J.S.

1. Burridge K, Chrzanowska-Wodnicka M (1996) Focal adhesions, contractility, and signaling. *Annu Rev Cell Dev Biol* 12:463–518.
2. Mege RM, Gavard J, Lambert M (2006) Regulation of cell–cell junctions by the cytoskeleton. *Curr Opin Cell Biol* 18(5):541–548.
3. Dawes-Hoang RE, et al. (2005) folded gastrulation, cell shape change and the control of myosin localization. *Development* 132(18):4165–4178.
4. Martin AC, Kaschube M, Wieschaus EF (2009) Pulsed contractions of an actin-myosin network drive apical constriction. *Nature* 457(7228):495–499.
5. Bertet C, Sulak L, Lecuit T (2004) Myosin-dependent junction remodelling controls planar cell intercalation and axis elongation. *Nature* 429(6992):667–671.
6. Rauzi M, Verant P, Lecuit T, Lenne PF (2008) Nature and anisotropy of cortical forces orienting Drosophila tissue morphogenesis. *Nat Cell Biol* 10(12):1401–1410.
7. Rolo A, Skoglund P, Keller R (2009) Morphogenetic movements driving neural tube closure in Xenopus require myosin IIB. *Dev Biol* 327(2):327–338.
8. Skoglund P, Rolo A, Chen X, Gumbiner BM, Keller R (2008) Convergence and extension at gastrulation require a myosin IIB-dependent cortical actin network. *Development* 135(14):2435–2444.
9. Conti MA, Even-Ram S, Liu C, Yamada KM, Adelstein RS (2004) Defects in cell adhesion and the visceral endoderm following ablation of nonmuscle myosin heavy chain II-A in mice. *J Biol Chem* 279(40):41263–41266.
10. Abraham S, et al. (2009) VE-Cadherin-mediated cell–cell interaction suppresses sprouting via signaling to MLC2 phosphorylation. *Curr Biol* 19(8):668–674.
11. de Rooij J, Kerstens A, Danuser G, Schwartz MA, Waterman-Storer CM (2005) Integrin-dependent actomyosin contraction regulates epithelial cell scattering. *J Cell Biol* 171(1):153–164.
12. Ivanov AI, et al. (2007) A unique role for nonmuscle myosin heavy chain IIA in regulation of epithelial apical junctions. *PLoS One* 2(7):e658.
13. Miyake Y, et al. (2006) Actomyosin tension is required for correct recruitment of adherens junction components and zonula occludens formation. *Exp Cell Res* 312(9):1637–1650.
14. Shewan AM, et al. (2005) Myosin 2 is a key Rho kinase target necessary for the local concentration of E-cadherin at cell–cell contacts. *Mol Biol Cell* 16(10):4531–4542.
15. Yamada S, Nelson WJ (2007) Localized zones of Rho and Rac activities drive initiation and expansion of epithelial cell–cell adhesion. *J Cell Biol* 178(3):517–527.
16. Gavard J, et al. (2004) Lamellipodium extension and cadherin adhesion: Two cell responses to cadherin activation relying on distinct signalling pathways. *J Cell Sci* 117(Pt 2):257–270.
17. Lambert M, et al. (2007) Nucleation and growth of cadherin adhesions. *Exp Cell Res* 313(19):4025–4040.
18. Bershadsky AD, Balaban NQ, Geiger B (2003) Adhesion-dependent cell mechanosensitivity. *Annu Rev Cell Dev Biol* 19:677–695.
19. Chen CS, Tan J, Tien J (2004) Mechanotransduction at cell–matrix and cell–cell contacts. *Annu Rev Biomed Eng* 6:275–302.
20. Bard L, et al. (2008) A molecular clutch between the actin flow and N-cadherin adhesions drives growth cone migration. *J Neurosci* 28(23):5879–5890.
21. Baumgartner W, et al. (2000) Cadherin interaction probed by atomic force microscopy. *Proc Natl Acad Sci USA* 97(8):4005–4010.
22. Baumgartner W, Schutz GJ, Wiegand J, Golenhofen N, Drenckhahn D (2003) Cadherin function probed by laser tweezer and single molecule fluorescence in vascular endothelial cells. *J Cell Sci* 116(Pt 6):1001–1011.
23. Chu YS, et al. (2004) Force measurements in E-cadherin-mediated cell doublets reveal rapid adhesion strengthened by actin cytoskeleton remodeling through Rac and Cdc42. *J Cell Biol* 167(6):1183–1194.
24. Ko KS, Arora PD, McCulloch CA (2001) Cadherins mediate intercellular mechanical signaling in fibroblasts by activation of stretch-sensitive calcium-permeable channels. *J Biol Chem* 276(38):35967–35977.
25. Kris AS, Kamm RD, Sieminski AL (2008) VASP involvement in force-mediated adherens junction strengthening. *Biochem Biophys Res Commun* 375(1):134–138.
26. Panorchan P, et al. (2006) Single-molecule analysis of cadherin-mediated cell–cell adhesion. *J Cell Sci* 119(Pt 1):66–74.
27. Potard US, Butler JP, Wang N (1997) Cytoskeletal mechanics in confluent epithelial cells probed through integrins and E-cadherins. *Am J Physiol* 272(5 Pt 1):C1654–1663.
28. Tan JL, et al. (2003) Cells lying on a bed of microneedles: An approach to isolate mechanical force. *Proc Natl Acad Sci USA* 100(4):1484–1489.
29. Balaban NQ, et al. (2001) Force and focal adhesion assembly: A close relationship studied using elastic micropatterned substrates. *Nat Cell Biol* 3(5):466–472.
30. Navarro P, et al. (1995) Catenin-dependent and -independent functions of vascular endothelial cadherin. *J Biol Chem* 270(52):30965–30972.
31. Dudek SM, Garcia JG (2001) Cytoskeletal regulation of pulmonary vascular permeability. *J Appl Physiol* 91(4):1487–1500.
32. McVerry BJ, Garcia JG (2004) Endothelial cell barrier regulation by sphingosine 1-phosphate. *J Cell Biochem* 92(6):1075–1085.
33. Shikata Y, Birukov KG, Garcia JG (2003) S1P induces FA remodeling in human pulmonary endothelial cells: Role of Rac, GIT1, FAK, and paxillin. *J Appl Physiol* 94(3):1193–1203.
34. Ehrlich JS, Hansen MD, Nelson WJ (2002) Spatio-temporal regulation of Rac1 localization and lamellipodia dynamics during epithelial cell–cell adhesion. *Dev Cell* 3(2):259–270.
35. Mehta D, Konstantoulaki M, Ahmmed GU, Malik AB (2005) Sphingosine 1-phosphate-induced mobilization of intracellular Ca2+ mediates rac activation and adherens junction assembly in endothelial cells. *J Biol Chem* 280(17):17320–17328.
36. Gao Y, Dickerson JB, Guo F, Zheng J, Zheng Y (2004) Rational design and characterization of a Rac GTPase-specific small molecule inhibitor. *Proc Natl Acad Sci USA* 101(20):7618–7623.
37. Ridley AJ, Paterson HF, Johnston CL, Diekmann D, Hall A (1992) The small GTP-binding protein rac regulates growth factor-induced membrane ruffling. *Cell* 70(3):401–410.
38. Nelson CM, et al. (2005) Emergent patterns of growth controlled by multicellular form and mechanics. *Proc Natl Acad Sci USA* 102(33):11594–11599.
39. Scott IC, Stainier DY (2003) Developmental biology: Twisting the body into shape. *Nature* 425(6957):461–463.
40. Ingber DE (2003) Tensegrity I. Cell structure and hierarchical systems biology. *J Cell Sci* 116(Pt 7):1157–1173.
41. Nelson CM, Pirone DM, Tan JL, Chen CS (2004) Vascular endothelial-cadherin regulates cytoskeletal tension, cell spreading, and focal adhesions by stimulating RhoA. *Mol Biol Cell* 15(6):2943–2953.
42. Parker KK, et al. (2002) Directional control of lamellipodia extension by constraining cell shape and orienting cell tractional forces. *FASEB J* 16(10):1195–1204.
43. Vestweber D (2000) Molecular mechanisms that control endothelial cell contacts. *J Pathol* 190(3):281–291.
44. Erez N, Bershadsky A, Geiger B (2005) Signaling from adherens-type junctions. *Eur J Cell Biol* 84(2–3):235–244.
45. Vasioukhin V, Bauer C, Yin M, Fuchs E (2000) Directed actin polymerization is the driving force for epithelial cell–cell adhesion. *Cell* 100(2):209–219.
46. Brevier J, Montero D, Svitkina T, Riveline D (2008) The asymmetric self-assembly mechanism of adherens junctions: A cellular push-pull unit. *Phys Biol* 5(1):016005.
47. Hall A (2005) Rho GTPases and the control of cell behaviour. *Biochem Soc Trans* 33(Pt 5):891–895.
48. Waschke J, et al. (2004) Requirement of Rac activity for maintenance of capillary endothelial barrier properties. *Am J Physiol-Heart C* 286(1):H394–401.
49. Kaibuchi K, Kuroda S, Fukata M, Nakagawa M (1999) Regulation of cadherin-mediated cell–cell adhesion by the Rho family GTPases. *Curr Opin Cell Biol* 11(5):591–596.
50. Ukropec JA, Hollinger MK, Salva SM, Woolkalis MJ (2000) SHP2 association with VE-cadherin complexes in human endothelial cells is regulated by thrombin. *J Biol Chem* 275(8):5983–5986.
51. Halir R, Flusser J (1998) Numerically stable direct least squares fitting of ellipses. *Proceedings of the 6th International Conference in Central Europe on Computer Graphics and Visualization* (WSCG, Plzen, Czech Republic), pp 125–132.